Muon spin relaxation studies of incommensurate magnetism and superconductivity in stage-4 $La_2CuO_{4.11}$ and $La_{1.88}Sr_{0.12}CuO_4$

A. T. Savici, Y. Fudamoto, I. M. Gat, T. Ito, M. I. Larkin, and Y. J. Uemura*
Department of Physics, Columbia University, New York, New York 10027

G. M. Luke
Department of Physics and Astronomy, McMaster University, Hamilton, Ontario, Canada L8P 4N3

K. M. Kojima
Department of Superconductivity, Faculty of Engineering, University of Tokyo, 7-3-1 Hongo, Tokyo 113-8656, Japan

Y. S. Lee and M. A. Kastner
Department of Physics, MIT, Cambridge, Massachusetts 02139

R. J. Birgeneau
Department of Physics, MIT, Cambridge, Massachusetts 02139
and Department of Physics, University of Toronto, Toronto, Ontario, Canada M5S 1A7

K. Yamada
Institute for Chemical Research, Kyoto University, Uji, Kyoto 611-0011, Japan
(Received 1 February 2002; published 16 July 2002)

We report muon spin relaxation (μSR) measurements using single crystals of oxygen-intercalated stage-4 $La_2CuO_{4.11}$ (LCO:4.11) and $La_{1.88}Sr_{0.12}CuO_4$ (LSCO:0.12), in which neutron scattering studies have found incommensurate magnetic Bragg reflections. In both systems, zero-field μSR measurements show muon spin precession below the Néel temperature T_N with frequency 3.6 MHz at $T\rightarrow 0$, having a Bessel function line shape, characteristic of spin-density-wave systems. The amplitude of the oscillating and relaxing signals of these systems is less than half the value expected for systems with static magnetic order in 100% of the volume. Our results are consistent with a simulation of local fields for a heuristic model with (a) incommensurate spin amplitude modulation with the maximum ordered Cu moment size of $\sim 0.36\mu_B$, (b) static Cu moments on the CuO_2 planes forming ''islands'' having typical radius 15–30 Å, comparable to the in-plane superconducting coherence length, and (c) the measured volume fraction of magnetic muon sites V_μ increasing progressively with decreasing temperature below T_N towards $V_\mu \sim 40\%$ for LCO:4.11 and 18% for LSCO:0.12 at $T\rightarrow 0$. These results may be compared with correlation lengths in excess of 600 Å and a long range ordered moment of $0.15\pm 0.05\mu_B$ measured with neutron scattering techniques. In this paper we discuss a model that reconciles these apparently contradictory results. In transverse magnetic field μSR measurements, sensitive to the in-plane magnetic field penetration depth λ_{ab}, the results for LCO:4.11 and LSCO:0.12 follow correlations found for underdoped, overdoped and Zn-doped high-T_c cuprate systems in a plot of T_c versus the superconducting relaxation rate $\sigma(T\rightarrow 0)$. This indicates that the volume-integrated value of n_s/m^* (superconducting carrier density / effective mass) is a determining factor for T_c, not only in high-T_c cuprate systems without static magnetism, but also in the present systems where superconductivity coexists with static spin-density-wave spin order.

DOI: 10.1103/PhysRevB.66.014524 PACS number(s): 74.25.Ha, 76.75.+i, 74.72.Dn, 75.25.+z

I. INTRODUCTION

The interplay between superconductivity and magnetism is one of the central issues of high-T_c superconductivity (HTSC), which has been extensively studied both experimentally and theoretically.[1] In particular, dynamic[2–8] and static[9–16] spin correlations with incommensurate wave vectors have been found by neutron scattering. These, as well as x-ray photoelectron studies,[17–19] have been discussed in terms of a ''stripe'' modulation of the spin and charge densities.[20–23] Yet it has not been clear whether static magnetism supports or competes with superconductivity, or if the magnetism and superconductivity coexist in the same microscopic regions of the CuO_2 planes or in different regions. While neutron measurements make it clear that long range magnetic order exists, the Bragg peak intensity integrates over the sample volume and is not, therefore, sensitive to microscopic spatial variations in the order parameter.

Muon spin relaxation (μSR) measurements[24,25] provide a complementary probe in this regard. In a magnetic material having a heterogenous structure, such as ''magnetic'' and ''nonmagnetic'' regions, μSR data are composed of two different signals, corresponding to different environments with signal amplitudes roughly proportional to their volume fractions. Local magnetic fields at muon sites result primarily from the dipolar interaction. In antiferromagnetically ordered

systems the local field decays very quickly with increasing distance from ordered spins, resulting in an effective range of the field of $\sim 10-15$ Å in cuprate systems. Thus, any heterogeneous magnetic structure in HTSC, having a length scale larger than this, should produce multiple and distinguishable μSR signals.

In this paper, we report zero-field (ZF) and transverse-field (TF) μSR measurements in a single crystal of $La_2CuO_{4.11}$ (LCO:4.11) where excess oxygen is intercalated in a stage-4 structure.[16] This system is superconducting below $T_c \sim 42$ K. Observation of sharp satellite Bragg peaks in neutron scattering indicates static long range (>600 Å) spin density wave (SDW) order below $T_N \sim 42$ K. The modulation wave vector of the SDW is comparable to those observed in $La_{2-x}Sr_xCuO_4$ (LSCO) and $La_{2-x-y}Nd_ySr_xCuO_4$ (LNSCO) systems with the hole concentration $x \sim 0.125$.[9,12] The LCO:4.11 system is especially interesting since (a) it has the highest superconducting T_c in the 214 family of materials, (b) it has a rather high magnetic T_N, which is very close to T_c, and well developed long range magnetic order below T_N, (c) there is no randomness arising from Sr substitution, and the intercalated oxygen ions are three dimensionally ordered. Preliminary results and analysis of our ZF-μSR in LCO:4.11 have been presented at a recent conference.[26]

We also report μSR results in a superconducting $La_{1.88}Sr_{0.12}CuO_4$ (LSCO:0.12) single crystal with $T_c \sim 30$ K which exhibits magnetic Bragg peaks in neutron scattering.[13] Comparing these results with those of a simulation of the local field distribution at possible muon sites, we examine various models for the magnetically ordered regions. The interplay between superconductivity and magnetism is discussed in the context of the superfluid density n_s/m^* derived from TF-μSR results.

μSR studies of magnetism in HTSC systems started in 1987 with studies of antiferromagnetic La_2CuO_4 (AF-LCO),[27] which provided the first evidence of static magnetic order. Subsequently, μSR studies on La_2CuO_4,[28] $(La,Li)_2CuO_4$,[29] $La_{2-x}Sr_xCuO_4$,[30–34] and $YBa_2Cu_3O_y$,[34,35] were performed to characterize magnetic phase diagrams as a function of hole concentration and also to study details of the spin glass states near $x=0.05$.

μSR measurements of HTSC systems with hole concentration x near 1/8 were first performed in $La_{1.875}Ba_{0.125}CuO_4$.[36] These detected static magnetic order below $T_N=32$ K and a Bessel function μSR line shape, characteristic of spin density wave systems. A reduction of T_c, associated with an increase of the muon spin relaxation due to quasi-static magnetism, was also found by μSR in $La_{2-x}Sr_xCuO_4$ near $x=0.12$.[37] Recent μSR studies on $(La,Nd,Sr)_2CuO_4$ (LNSCO),[38,39] $(La,Eu,Sr)_2CuO_4$ (LESCO),[40,41] and $La_{1.875}Ba_{0.125-y}Sr_yCuO_4$ (LBSCO) (Ref. 42) found the characteristic Bessel function line shape with the same frequency $\nu \sim 3.5$ MHz in all these systems. In the latter studies the primary emphasis was determining the magnetic phase diagram as a function of rare-earth and hole concentrations. Although the existence of ''zero/low field muon sites,'' expected for decomposition of the system into regions with and without static magnetic order, was discussed in these reports,[40,42] a systematic study of magnetic volume fraction was not made.

Previously, Pomjakushin *et al.*[43] reported a μSR study for single crystal specimens of La_2CuO_{4+y} doped with oxygen, with $y=0.02$ (LCO:4.02) and 0.04 (LCO:4.04), which have compositions in the miscibility gap between AF-LCO and the stage-6 superconducting compound. In zero field, they observed μSR precession signals identical to those found in AF-LCO. With decreasing temperature in LCO:4.02, the amplitude of this oscillatory signal increased from nearly zero above the superconducting $T_c \sim 15$ K to more than a half of that in AF-LCO at $T \to 0$. In LCO:4.04, the oscillatory signal appeared below $T \sim 230$ K with an amplitude corresponding to approximately a 10% volume fraction for the AF region, and then exhibited a sharp increase below the superconducting $T_c \sim 25$ K to about a half volume fraction at $T \to 0$. In both cases, the amplitudes of the AF oscillation exhibited an increase below T_c. The diamagnetic susceptibility of the LCO:4.02 specimen was, however, destroyed by a small applied field, indicating rather fragile superconductivity. Lack of information about the crystal orientation in the μSR measurements prevented a reliable estimate of the volume fraction in this study.

In Sec II we present experimental details and results of the ZF-μSR measurements. Section III contains our simulation based on a model in which the sample contains microscopic regions where there is full magnetic order and other microscopic regions where the magnetic fields are too small to cause muon precession. In Sec. IV we present results of measurements in a transverse magnetic field that are sensitive to the superconductivity. Finally in Sec. V we discuss the results and draw conclusions.

II. ZERO FIELD μSR MEASUREMENTS

Single crystals of LCO:4.11 and LSCO:0.12 have been prepared as described in Refs. 16 and 13, which report neutron scattering studies of these crystals, respectively. The excess-oxygen doped La_2CuO_{4+y} sample is prepared by electrochemically doping a single crystal of pure La_2CuO_4 which is grown by the traveling solvent floating-zone method. The crystal has a mass of 4.21 grams and is cylindrical in shape. As a result of twinning, there are equal populations of two twin domains with either the *a* or *b* crystallographic axis (in orthorhombic notation) nearly parallel to the cylinder's long axis. In both twin domains, the *c* axis is perpendicular to the long axis. Thermogravitimetric analysis on our samples has been performed on two smaller La_2CuO_{4+y} crystals with $T_c=42$ K. We find oxygen concentrations of $y=0.10(1)$ and $y=0.12(1)$. The large crystal has the same T_c, so its oxygen concentration is expected to correspond to $y=0.11(1)$.

Neutron diffraction measurements have shown that this material has a structural modulation along the *c* axis corresponding to stage-4.[16] Further details regarding the characterization of the stage-4 crystal by neutron scattering, susceptibility, and transport techniques may be found in Refs. 16 and 44.

μSR measurements were performed at TRIUMF, using a surface muon beam with an incident muon momentum of 28 MeV/c, following the standard procedure described in Refs. 24 and 25. We employed the so-called ''low-background'' muon spectrometer, which has the capability of vetoing events from muons landing in areas other than the specimen, to ensure much less than $\sim$10% background signal in our μSR data. In ZF-μSR, we observed positron time spectra via counters placed forward (F) and backward (B) to the incident beam direction ($\hat{z}$), with the polarization of incident muons $\vec{P}_\mu$ antiparallel to $\hat{z}$. The muon spin relaxation function $G_z(t)$ was obtained from forward (F) and backward (B) time spectra as

$$G_z(t)=[B(t)-F(t)]/[F(t)+B(t)], \tag{1}$$

after correcting for the difference in effective solid angles of the F and B counters. As illustrated in Fig. 1(a), two sets of measurements were made with the c axis of the specimen mounted parallel (configuration CZ-I) and perpendicular (CZ-II) to $\hat{z}\|\vec{P}_\mu$.

Figures 2(a) and 2(b) show the muon spin polarization function $G_z(t)$ observed in these two crystals for CZ-I and CZ-II. Also included are the results obtained for ceramic specimens of nonsuperconducting $La_{1.875}Ba_{0.125}CuO_4$ (LBCO:0.125) (Ref. 36) and $La_{1.475}Nd_{0.4}Sr_{0.13}CuO_4$ (LNSCO:0.13).[38]

We see almost no relaxation above T_N in the time range $t\leqslant 1$ μs. Below $T_N\sim 42$ K of LCO:4.11 and $T_N\sim 20$ K of LSCO:0.12, a small oscillatory component appears, with a Bessel-function line shape characteristic of muon precession in SDW systems.[45,46] The amplitude A_{or} of this oscillating and relaxing signal is limited to about 34% (CZ-I) and 24% (CZ-II) at $T\rightarrow 0$ for LCO:4.11, and 20% (CZ-I) and 10% (CZ-II) for LSCO:0.12. If we define the internal field at a muon site as $\vec{H}$ and θ is the angle between $\hat{z}$ and $\vec{H}$, as illustrated in Fig. 1(b), the oscillatory/relaxing amplitude represents $\sin^2(\theta)$ averaged over all the muon sites. In a ceramic specimen which undergoes magnetic order in 100% of the volume, this amplitude is 67% ($=2/3$), as shown in the case of LBCO:0.125. Therefore, the observed signal amplitudes $A_{\rm or}$ for LCO:4.11 and LSCO:0.12 are less than half the value expected for a sample with a SDW uniformly established throughout its volume.

In single-crystal specimens, $A_{\rm or}$ can have a small value if the local fields $\vec{H}$ for the majority of muon sites are parallel to $\hat{z}\|\vec{P}_\mu$. For this case, however, one should see a large $A_{\rm or}$ when the crystal orientation is rotated by 90° from CZ-I to CZ-II or vice versa. Thus, our results, with small $A_{\rm or}$ values for the both configurations, cannot be attributed to such anisotropy. In view of the symmetry of the LCO and LSCO structures, the ''powder average'' value of $A_{\text{or-pwd}}$ can be obtained[26] as

$$A_{\text{or-pwd}}\equiv(1/3)\times[A_{\text{or:CZ-}I}+2A_{\text{or:CZ-}II}], \tag{2}$$

which yields 27% for LCO:4.11 and 12% for LSCO:0.12. The reduction of $A_{\text{or-pwd}}$ from 66.7% indicates the existence of ''zero/low-field'' muon sites.

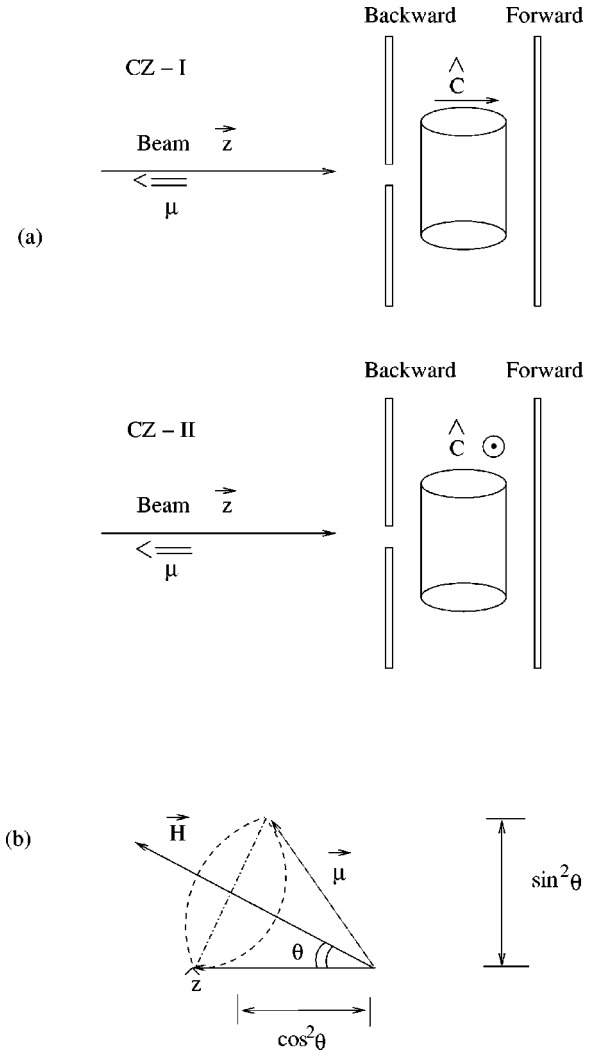

FIG. 1. (a) Schematic view of the experimental configurations in zero field μSR (ZF-μSR) employed in the present study, with the initial muon spin polarization parallel (CZ-I) and perpendicular (CZ-II) to the $\hat{c}$ axis of the single crystal specimen. (b) The oscillating part of the muon polarization signal, proportional to $\sin^2(\theta)$, and the nonoscillating part to $\cos^2(\theta)$, where θ is the angle between the local magnetic field and the initial muon spin direction.

We have analyzed the ZF-μSR data by fitting the results at $t\leqslant 1\,\mu$s to

$$G_z(t)=A_{\rm or}j_0(\omega t)\exp(-\Lambda t)+A_n\exp[-\Delta^2t^2/2], \tag{3}$$

where j_0 is the zeroth order Bessel function and A_n represents the nonoscillating amplitude. The first exponential term represents the damping of the Bessel oscillation, whereas the second describes the slow decay due to nuclear dipolar fields. We obtain the volume fraction V_μ of muon sites that experience the SDW field using

$$V_\mu\equiv A_{\text{or-pwd}}/(2/3), \tag{4}$$

with $A_{\text{or-pwd}}$ determined from Eq. (2) at the lowest temperature. We then scale the values for higher temperatures using $A_{\rm or}$ results for the CZ-I configuration. For our fit range of t

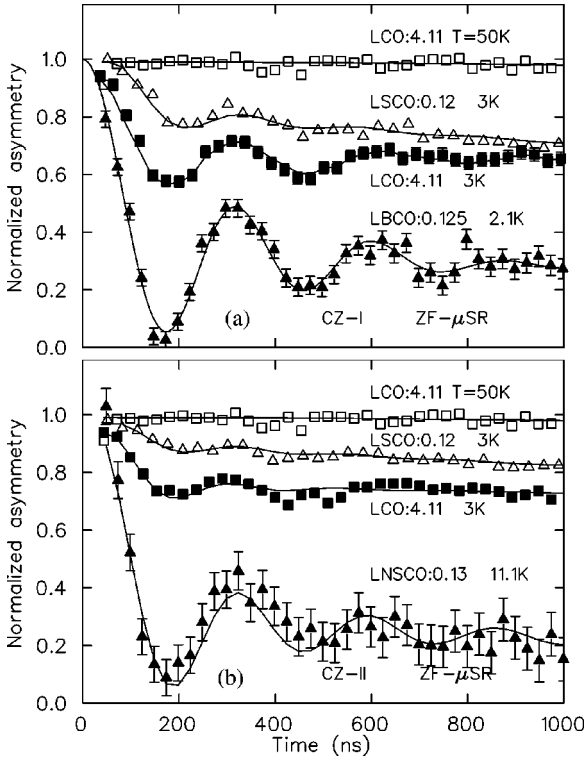

FIG. 2. Time spectra of the muon spin polarization observed by ZF-μSR with (a) the CZ-I configuration and (b) the CZ-II configuration for $La_2CuO_{4.11}$ (LCO:4.11) and $La_{1.88}Sr_{0.12}CuO_4$ (LSCO:0.12). Also included are the results for ceramic specimens of $La_{1.875}Ba_{0.125}CuO_4$ (LBCO:0.125) from Ref. 36 and $La_{1.47}Nd_{0.4}Sr_{0.13}CuO_4$ (LNSCO:0.13) from Ref. 38.

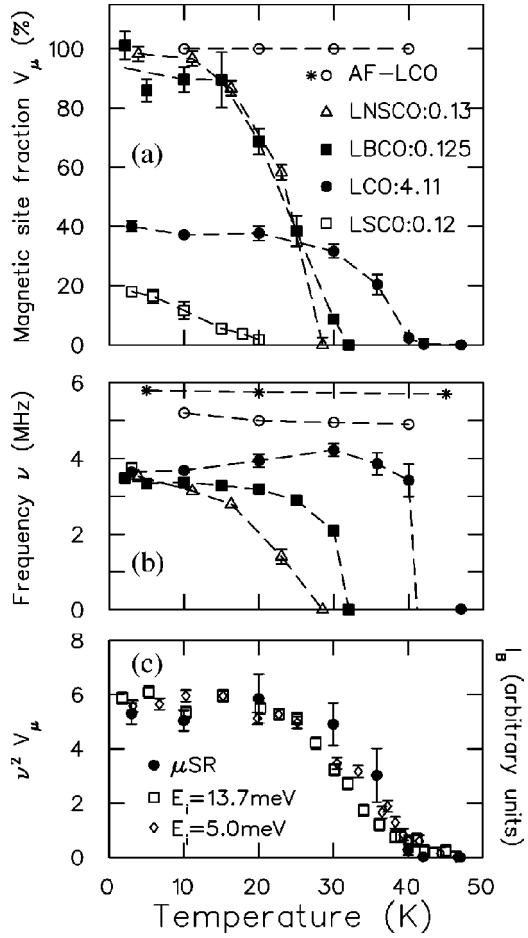

FIG. 3. (a) Volume fraction V_μ of muon sites with a static magnetic field larger than $\sim$30 G and (b) frequency of the precessing signal in $La_2CuO_{4.11}$ (LCO:4.11) and $La_{1.88}Sr_{0.12}CuO_4$ (LSCO:0.12) (from the present study), compared with the results in $La_{1.875}Ba_{0.125}CuO_4$ (LBCO:0.125) (Ref. 36), $La_{1.47}Nd_{0.4}Sr_{0.13}CuO_4$ (LNSCO:0.13) (Ref. 38), and antiferromagnetic $La_2CuO_{4+\delta}$ (AF-LCO) (Refs. 27 and 28). The broken lines are guides to the eye. (c) Comparison of the neutron Bragg peak intensity I_B in $La_2CuO_{4.11}$ (LCO:4.11) (Ref. 16) with those expected from the μSR results (present study) as $I_B \propto V_\mu \times \nu^2$. μSR and neutron results are scaled using the values near $T \rightarrow 0$.

$\leqslant 1$ μs, those muon sites with $H \geqslant 30$ G contribute to the first term in Eq. (3), and thus are identified as ''finite-field muon sites.''

Figures 3(a) and 3(b) show the temperature dependence of V_μ and the oscillation frequency $\nu = \omega/2\pi$ for LCO:4.11, LSCO:0.12, LBCO:0.125,[36] and LNSCO:0.13 (ceramic).[38] The common Bessel-function line shape and the nearly identical frequency $\nu \sim 3.5$ MHz (corresponding to maximum internal field of 260 G) at $T \rightarrow 0$ for all the four systems indicate that the spin configurations and magnitudes of the static Cu moments (proportional to ν) surrounding the ''finite-field muon sites'' are identical for all the four systems. The volume fraction V_μ increases progressively below T_N with decreasing temperature, in both LCO:4.11 and LSCO:0.12. The frequency ν acquires its full value just below T_N in LCO:4.11. In Fig. 3(c), we compare the temperature dependence of the neutron Bragg-peak intensity I_B of LCO:4.11 (Ref. 16) with $V_\mu \times \nu^2$ from μSR. The good agreement of neutron and muon results indicate that these two probes detect the same static magnetism even though the former measures the ordered moment over distances $\geqslant 600$ Å. The μSR results suggest that the observed temperature dependence of I_B should be ascribed mainly to the change of the site fraction containing ordered Cu spins, rather than to the increase of the static moment on individual Cu atoms although this is model dependent.

To illustrate further this unusual temperature dependence of the magnetic order parameter in LCO:4.11, we compare ZF-μSR spectra of LCO:4.11 and AF-LCO ($T_N \geqslant 250$ K) in Fig. 4. In AF-LCO [Fig. 4(b)], as in most conventional magnetic systems where long-range magnetic order develops in 100% of the volume, ZF-μSR data exhibit muon spin precession whose amplitude is nearly independent of temperature, but whose frequency increases with decreasing temperature. In contrast, for LCO:4.11 [Fig. 4(a)] the oscillation amplitude increases gradually with decreasing temperature below T_N while the frequency just below T_N is already close to the low-temperature value. This implies that in LCO:4.11 the local order is well developed but dynamic above T_N, and the ordering process below T_N involves the ordering of this local magnetism over long distances with a concomitant freezing of the spins.

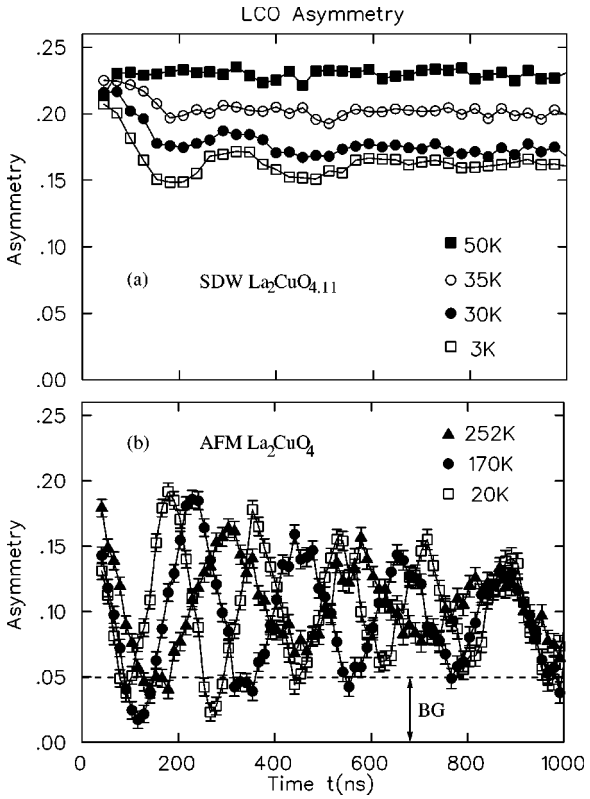

FIG. 4. Time spectra of ZF-μSR measurements in (a) LCO:4.11 and (b) AF-LCO. The amplitude of the oscillating and relaxing signal varies in (a) below T_N without much change in the frequency, while in (b) the amplitude does not depend on T and the frequency increases with decreasing T. The latter behavior is observed in ZF-μSR of many conventional magnetic systems. The spectrum (a), obtained by using a low-background μSR spectrometer, has the background signal level below 0.01 in asymmetry. The spectrum (b), obtained in 1987 by using an older apparatus, has the expected background level shown by the broken line (BG).

III. SIMULATION OF ZERO-FIELD μSR

To explore the possible origin of the two kinds of muon sites, we have performed computer simulations of the local field distributions at possible muon sites. The location of the muon site in AF-LCO has been approximated by Hitti *et al.*[47] to be about 1 Å away from the apical oxygen, based on the expected length of the O^{2-}-μ^+ hydrogen bond. We have improved their estimate by taking into account the tilt of the CuO_6 octahedra and by comparing the observed μSR precession frequency $\nu=5.8$ MHz with the Cu long-range ordered moment size $0.55\mu_B$ in AF-LCO.[16] Figure 5 shows the location of the apical-oxygen muon site at $(0.199d,0d,0.171c)$ in the unit cell with $d=3.779$ Å and $c=13.2$ Å assumed in this simulation. Since the direction of $\vec{H}$ is very sensitive to a small change of the tilt angle of the CuO_6 octahedra, we calculate the expected ZF-μSR line shape for the powder average.

Figure 6(a) shows the line shape for this apical-oxygen muon site for (1) a 100% volume fraction of antiferromagnetically (AF) ordered Cu moments having modulation vector $k_{\rm AF}$ with ordered moment of $0.55\mu_B$ (chain-dotted line) and (2) Cu spins with an incommensurate SDW amplitude modulation superimposed on the antiferromagnetic correlations, with a maximum static Cu moment value of $0.35\mu_B$ (broken line). Here we have assumed that the SDW propagation vector is along the Cu-O-Cu bond direction (i.e., 45° to the orthorhombic a and b axes) with magnitude $k=2\pi/d\times0.12$ ($d=3.78$ Å is the distance between nearest-neighbor Cu atoms) We have calculated the spin polarization using

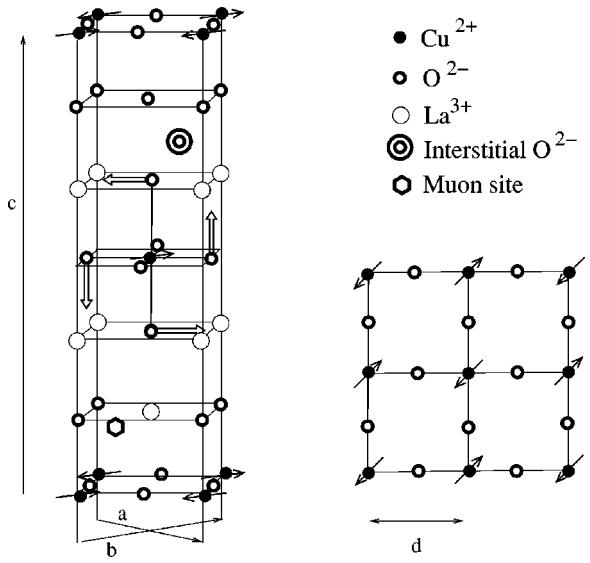

FIG. 5. Crystal structure of La_2CuO_4, shown with the positions of intercalated interstitial oxygen and the assumed muon site at (0,0.751,2.257) Å within the unit cell near an apical oxygen. The arrows attached to O^{2-} in the center of the figure show the direction of tilting (about 5°) of the CuO_6 octahedra.

$$\cos(\vec{k}_{\rm AF}\vec{x})\times\cos(\vec{k}\vec{x})=(1/2)\cos[(\vec{k}_{\rm AF}+\vec{k})\vec{x}]+(1/2)\cos[(\vec{k}_{\rm AF}-\vec{k})\vec{x}] \quad (5)$$

at a given position $\vec{x}$. These results confirm that the SDW model gives a line shape nearly identical to a Bessel function (solid line). In AF-LCO the observed μSR results[27,47] show a substantial damping of the sinusoidal precession, due to various possible origins, such as nuclear dipolar fields, variations of the muon site or crystal imperfection. To account for the reduction of the observed μSR frequency from 5.8 MHz in AF-LCO to 3.64 MHz at $T\rightarrow0$ in LCO:4.11, we need to assume that the maximum static Cu moment size in the SDW modulation is $\sim0.36\mu_B$. This may be compared with the bare Cu moment of $1.1\mu_B$.

Since there is a substantial density of intercalated oxygen in LCO:4.11, we have also modeled the field distribution at several locations 1 Å away from the expected site of the intercalated oxygen atoms. As may be seen from Fig. 6(b), which displays decay curves calculated for 100% ordered SDW Cu moments with maximum moment size of $0.35\mu_B$, there is no muon site location having zero or low internal field. Therefore, we cannot ascribe the existence of ''zero/

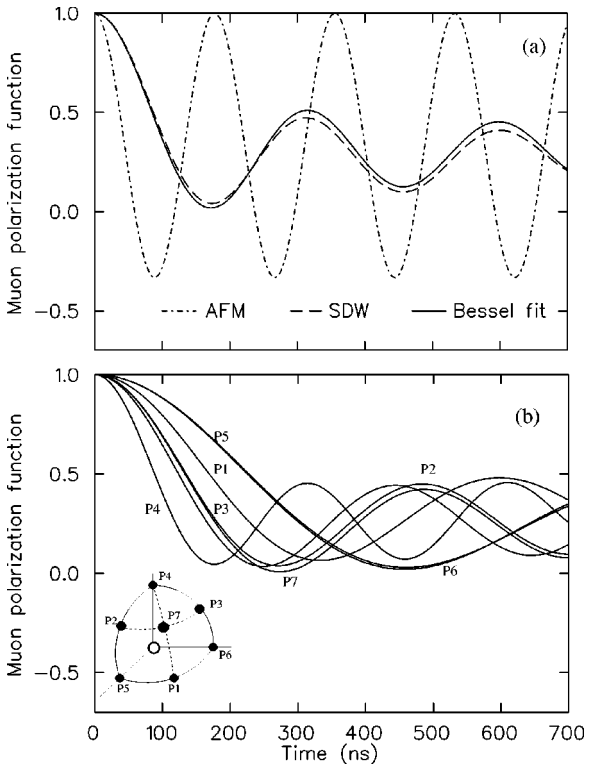

FIG. 6. Simulation results of the muon spin polarization functions in La_2CuO_4 obtained for static magnetic order involving all the Cu moments. An angular average is taken to represent the results for ceramic specimens. (a) Results for the muon site near the apical oxygen (see Fig. 5). The dotted line corresponds to the case with antiferromagnetic (AFM) spin correlations with the static Cu moment of $0.55\mu_B$, while the dashed line to the case with an SDW amplitude modulation with maximum static Cu moment of $0.35\mu_B$ and modulation wave vector $k=0.12\times 2\pi/d$ ($d=3.779$ Å) superimposed on the AFM correlations. The solid line shows a fit to a Bessel function. (b) Results for several hypothetical muon sites near the intercalated interstitial oxygen, illustrated in the inset, obtained for the above-mentioned SDW spin correlations.

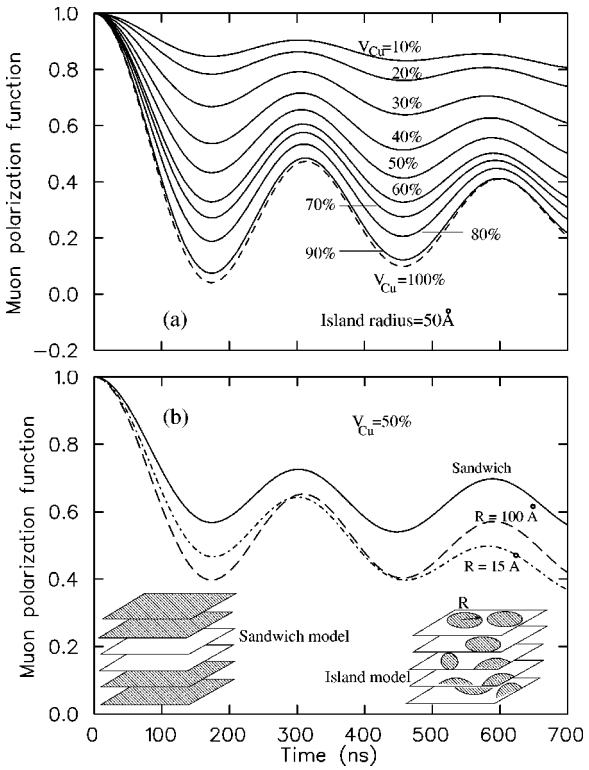

FIG. 7. Simulation results of the expected muon spin polarization functions for ceramic specimens of La_2CuO_4, obtained for the muon site near the apical oxygen and an SDW modulation with a maximum static Cu moment of $0.35\mu_B$ and modulation vector $k=0.12\times 2\pi/d$. (a) corresponds to magnetic island model where the Cu moments in a volume fraction V_{Cu} order with the SDW amplitude modulation, forming islands of radius $R=50$ Å, while the remaining Cu moments are not involved in static order. (b) The results for the magnetic island model with $R=15$ and 100 Å and for the ''sandwich model'' where two CuO_2 planes adjacent to the intercalated oxygen layer do not have any static Cu moments while all the Cu moments on the other two planes are ordered. All three curves shown in (b) correspond to $V_{Cu}=50\%$. The insets illustrate these two models, with the shaded regions containing SDW modulated static Cu moments and the blank regions without static Cu moments.

low-field sites'' in LCO:4.11 to intercalated oxygen. Furthermore, in LSCO:0.12, there is, of course, no intercalated oxygen, so it seems clear that the nonmagnetic sites must have a different origin.

In Fig. 7(a), we show the line shape $G_z(t)$ calculated for Cu moments in circular islands of SDW order in the CuO_2 planes, for various volume fractions V_{Cu} of static Cu spins, assuming the radius R of the circular islands to be $R\sim 50$ Å. Bessel function line shapes are obtained with a common frequency, while the regions without static Cu moments account for the zero-field sites. The size of the magnetic island is reflected in the dampening of the Bessel oscillation.

In Fig. 7(b) we compare the results of simulations for two different geometries. One is for circular magnetic islands with $V_{Cu}=50\%$ and $R=15$ and 100 Å. The other corresponds to an ''ordered sandwich'' model, where two out of every four CuO_2 planes contain completely ordered SDW Cu spins while the other two planes, presumably those adjacent to the intercalated O layers, have no static Cu spins. The curve for $R=15$ Å islands shows a fast dampening of the Bessel oscillation, together with a slow decay of the nonoscillating signal. In contrast, the curves for $R=100$ Å islands and for the sandwich model exhibit a long-lived Bessel oscillation, with little decay of the nonoscillating signal.

After generating line shapes for the SDW-island model, we have fitted the simulation results to the functional form of Eq. (3). Figure 8(a) shows the resulting magnetic site fraction V_μ as a function of volume fraction containing static Cu spin order V_{Cu}. We see that V_μ increases linearly with increasing Cu fraction, with a slope that is independent of island size R. The site fraction V_μ becomes nearly 100% at $V_{Cu}\sim 75\%$. This implies that even the observation of a magnetic μSR signal corresponding to $V_\mu=100\%$ cannot rule out the existence of regions of nonordered Cu moments in $\sim 25\%$ of the volume. By using the relationship between V_μ

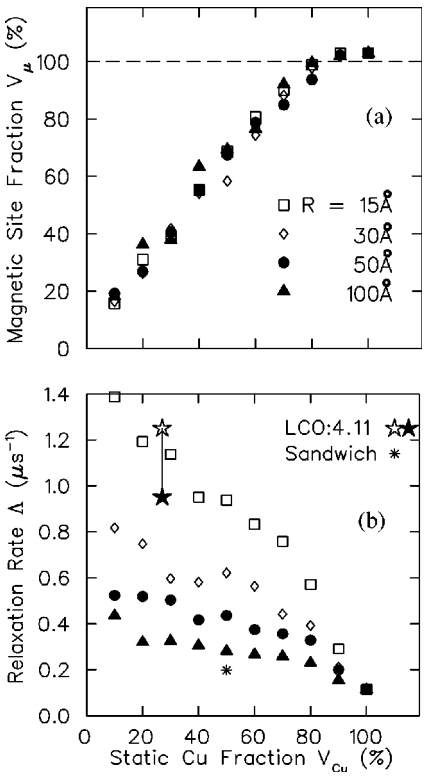

FIG. 8. (a) The volume fraction V_μ of muon sites with a static magnetic field larger than ~30 G, calculated in simulation as a function of the volume fraction V_{Cu} of the static Cu moment. (b) The relaxation rate Λ of the Bessel function oscillation, obtained by fitting the simulation results with Eq. (3), plotted as a function of V_{Cu}. The experimental results for LCO:4.11 (Raw data $\Lambda_{4.11}$ shown by an open star symbol and corrected data $\Lambda^c_{4.11}$ by a closed star symbol) allows estimation of the size of magnetic islands. The asterisk shows the relaxation rate Λ expected for the sandwich model.

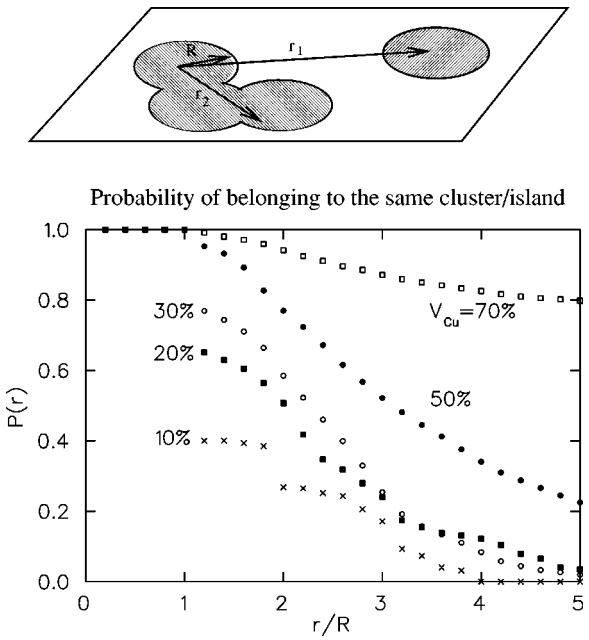

FIG. 9. Probability $P(r)$ that Cu spins belong to a certain cluster versus the distance from the center of an of radius R in the cluster. We assume that all the spins in a given island are correlated, and the correlation extends if there is any small overlap between adjacent islands on a given CuO_2 plane, as illustrated in the upper figure. For example, a Cu spin at a distance r_2 contributes "1.0" for the probability, while that at r_1 gives "0.0" contribution. We average over all the possible cluster/island configurations to calculate $P(r)$.

and V_{Cu}, we estimate as lower limits $V_{\mathrm{Cu}}\sim 27\%$ for our crystal of LCO:4.11 and ~10% for LSCO:0.12. Of course, this same possible difference between V_μ and V_{Cu} applies in all other copper oxide SDW systems.

In Fig. 8(b), we show the dampening rate Λ of the Bessel function oscillation. We find that a smaller radius R of the island results in a larger Λ. We also fit the observed spectra in LCO:4.11 with Eq. (3) and plot the corresponding point in Fig. 8(b) (open star symbol). The result $\Lambda_{4.11}=1.25\mu\mathrm{s}^{-1}$ agrees well with the simulation for $R=15$ Å. In actual systems, however, additional factors cause dampening of the Bessel oscillation, such as variations in the muon site, nuclear dipolar fields, and the effects of imperfections.

To account for these additional effects, we have fit the spectrum of AF-LCO at $T=20$ K in Fig. 4(b) with the simple form $\cos(\omega t+\phi)$ multiplied by an exponential decay $\exp(-\Lambda t)$, and obtain $\Lambda_{\mathrm{AF}}\sim 0.81\mu s^{-1}$. Assuming that Λ_{AF} represents the additional relaxation contributions, we have obtained a corrected relaxation rate from

$$\Lambda^c_{4.11}\equiv(\Lambda^2_{4.11}-\Lambda^2_{\mathrm{AF}})^{1/2}. \tag{6}$$

That is, we assume that the decay constants add in quadrature.

$\Lambda^c_{4.11}$ is shown by the closed star symbol in Fig. 8(b). These considerations lead us to estimate $R=15$–30 Å for the average radius of the static magnetic islands in LCO:4.11. A similar analysis for LSCO:0.12 would give roughly the same estimate for R. However, because the oscillation amplitude in LSCO:0.12 is much smaller than that in LCO:4.11, the analysis would be less reliable.

It is also possible to obtain the relaxation rate expected for the sandwich model. The result ($\Lambda=0.2\,\mu s^{-1}$), shown in Fig. 8(b) by the asterisk symbol, indicates that this model is less successful than the magnetic island model in reproducing the relaxation $\Lambda^c_{4.11}$ observed in LCO:4.11.

We now discuss a simple heuristic model for the propagation of magnetic order between these presumed islands. If we assume that spins in neighboring islands in the same CuO_2 plane are correlated when there is any overlap in the islands' area, as illustrated in Fig. 9 we can estimate the effective correlation length of the spin order. For various values of V_{Cu} we have calculated the probability that the direction of the Cu spins in the magnetic islands, located at a distance r from a Cu spin in the center of a magnetic island, is correlated with the direction of the Cu spin at $r=0$. The results of this calculation, shown in Fig. 9, suggest that even with the assumption that the spins are in islands, the order in a given plane may nevertheless propagate over long distances. However, for $V_{\mathrm{Cu}}=30\%$ the correlation length from Fig. 9 is only ~3 times the size of the magnetic island, whereas the narrow SDW peaks observed in neutron scattering measurements indicate that the static spins are correlated

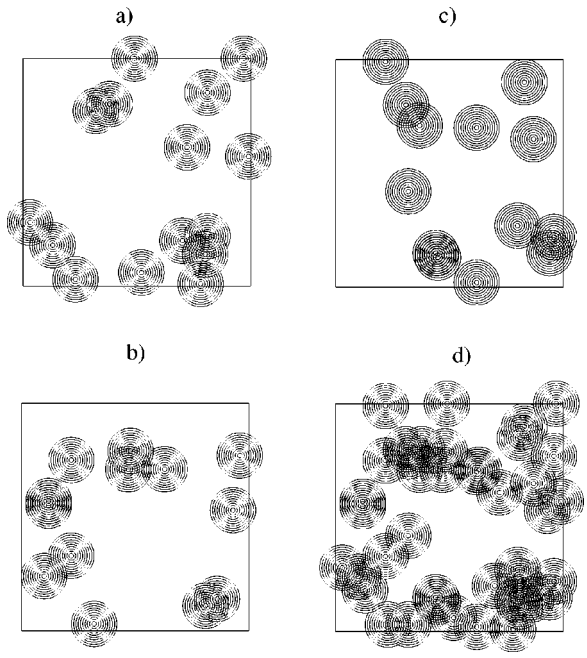

FIG. 10. Illustration of percolating cluster islands. (a)–(c) show planes with random locations of magnetic islands having integrated area fraction of 30%. (d) shows the overlap of (a)–(c). (d) demonstrates that most of the islands belong to the percolating cluster if we allow correlations of spins in ''overlapping islands'' on all the three planes.

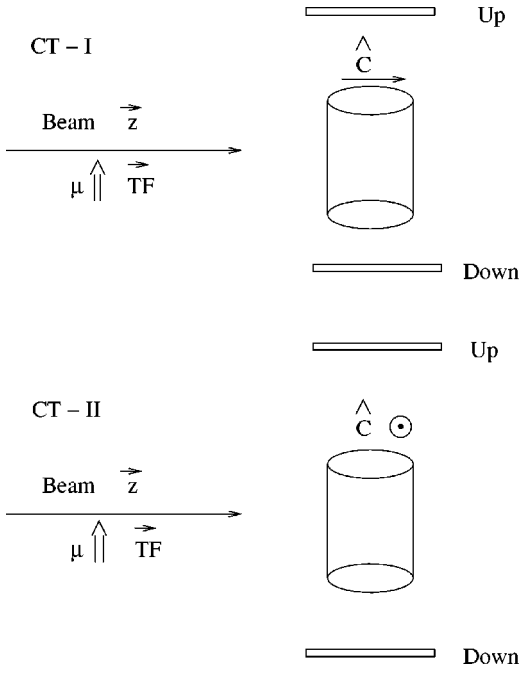

FIG. 11. Schematic view of experimental configurations of transverse field μSR (TF-μSR) measurements employed in the present work with the external field applied parallel (CT-I) and perpendicular (CT-II) to the $\hat{c}$ axis of the single crystal.

over very large distances (>600 Å) within the plane.[16] Therefore, some additional mechanism to increase the connectivity is required.

The results in Fig. 9 are obtained assuming no spin correlations between magnetic islands belonging to different neighboring CuO_2 planes. The neutron measurements of LCO:4.11 (Ref. 16) indicate that the static SDW order exhibits short range correlations along the *c* axis direction with a correlation length of ~ 13 Å, somewhat larger than twice the distance between adjacent CuO_2 planes. Such spin correlations along the *c* axis direction would further increase the size of the correlated clusters shown in Fig. 9. For example, if we allow correlations when any overlap exists among areas of the islands projected to the adjacent island on neighboring planes, the effective number of islands contributing to the ''connectivity'' would increase at least by three times compared to the case without interplane correlations. This is because all the islands on a given CuO_2 plane plus those on the upper and lower planes would participate in the correlations.

In Fig. 10, we illustrate this by showing randomly positioned islands of 30% integrated area fraction in three different planes (a)–(c). When we overlap these planes, almost all the islands achieve percolation, as shown in Fig. 10(d). Moreover, there could be further contribution from islands on the second neighbor planes which would enhance connectivity within the first neighbor planes. In this way, we expect a strong tendency towards percolation of spin correlations among randomly positioned magnetic islands.

IV. SUPERCONDUCTING PROPERTIES

TF-μSR measurements allow us to derive the magnetic field penetration depth λ from the superconducting contribution σ of the muon spin relaxation rate as $\sigma \propto \lambda^{-2} \propto n_s/m^*$ (superconducting carrier density/effective mass). This rate σ reflects the inhomogeneity of the magnetic field in the flux vortex structure, which varies over a length scale of ~ 1000–3000 Å. Any heterogeneity in the superconducting properties at length scales shorter than this will be averaged out. Thus, μSR probes superconductivity with a ~ 100 times coarser spatial resolution than that with which it probes static magnetism. In HTSC systems without any static magnetic order, the line shapes in TF-μSR spectra can be used to study more detailed spatial features, such as the size of the vortex core region.[48] In the present case, with co-existing superconductivity and static magnetic order, however, detailed line-shape analyses become very difficult.

We have performed TF-μSR measurements by rotating the incident muon polarization to be perpendicular to the beam $\vec{P}_\mu \perp \hat{z}$ and applying an external field parallel to $\hat{z}$ with the *c* axis of the specimen mounted either parallel to $\hat{z}$ (configuration CT-I) or perpendicular to $\hat{z}$ (configuration CT-II), as illustrated in Fig. 11. The muon spin polarization function $G_x(t)$ is measured using two sets of counters placed up (U) and down (D) of the incident beam.

As shown in Figs. 12(a) and 12(b), we observe a larger relaxation in CT-I, the geometry reflecting the in-plane penetration depth λ_{ab}, than in CT-II. We have analyzed the TF-μSR results by assuming the existence of a static internal

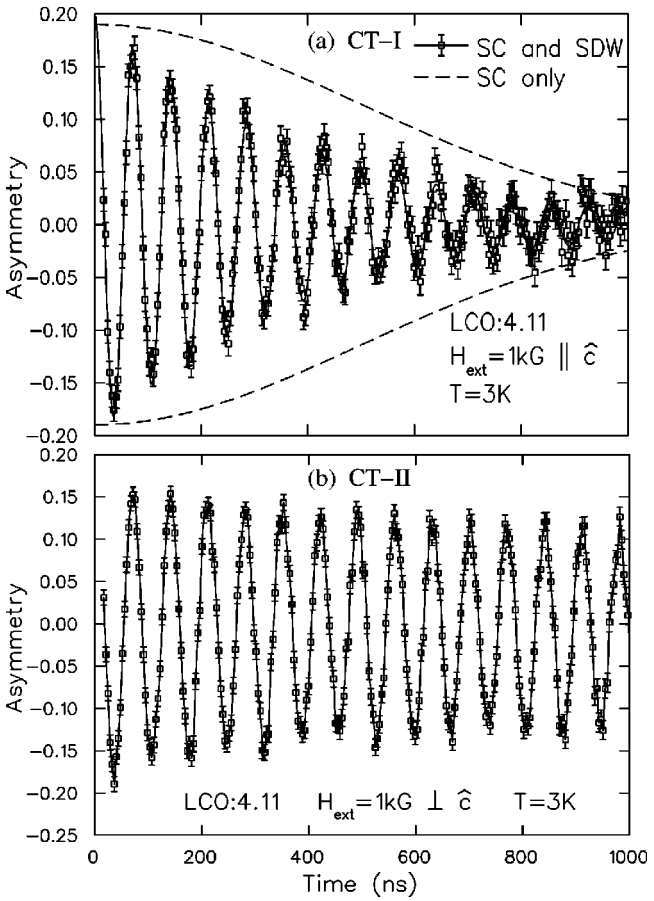

FIG. 12. Time spectra of the muon spin polarization observed in TF-μSR in LCO:4.11 obtained using (a) CT-I and (b) CT-II configurations. (a) shows faster damping than (b), reflecting the shorter penetration depth for the external field applied perpendicular to the CuO_2 planes. The effect from superconductivity alone is shown by the dotted line in (a), while the additional effect from static magnetism, multiplied to the dotted line, results in the observed relaxaion.

field in a volume fraction V_μ of muon sites, having the distribution in magnitude and direction estimated from the ZF-μSR measurements. We have then added vectorially the external field, with a Gaussian broadening due to superconductivity. For the ''zero/low-field muon sites'' with volume fraction (1-V_μ), we assume that the muon sees only the nuclear dipolar fields and the Gaussian-broadened external field. We fit the observed data with this model, and derive the Gaussian half width at half maximum of the superconducting contribution equal to σ/γ_μ. Figure 12(a) shows the calculated contributions to the relaxation from superconductivity and static magnetism, separately.

The temperature dependence of σ, observed in the CT-I configuration, is shown in Fig. 13 for LCO:4.11 and LSCO:0.12. The relaxation rate shows a gradual increase with decreasing temperature below T_c. To compare the values of $\sigma(T\rightarrow 0)$ with those observed in ceramic specimens of other HTSC systems,[49–52] we multiply by 1/1.4 to account for the effect of the anisotropic penetration depth.[53] We then add the corresponding points to the plot of $\sigma(T\rightarrow 0)$ versus T_c in Fig. 14. The points for the present systems lie on the

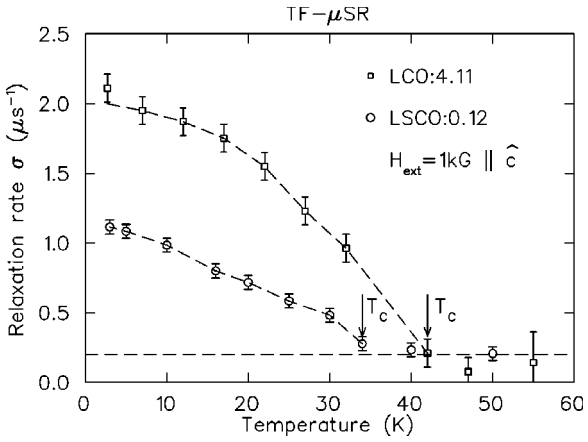

FIG. 13. Temperature dependence of the superconducting relaxation rate σ due to superconducting flux vortices, observed in TF-μSR measurements (with the CT-I configuration) in $La_2CuO_{4.11}$ (LCO:4.11) and $La_{1.88}Sr_{0.12}CuO_4$ (LSCO:0.12). The broken lines are guides to the eye.

same trajectory as other LSCO systems. We have also included a point for LESCO (Eu0.1, Sr0.15; ceramic), which exhibits static magnetic order with $V_\mu \sim 50\%$.[40,54,55] This point again falls on the trajectory. The correlation in Fig. 14 suggests that $\sigma \propto n_s/m^*$ at $T\rightarrow 0$ is a determining factor for T_c in HTSC systems with static stripe freezing (present systems and LESCO) in a way similar to the case for underdoped,[49,50] Zn-doped,[52] and overdoped[51,56] HTSC systems.

V. DISCUSSION AND CONCLUSIONS

A. Interplay between magnetic and superconducting volumes

Comparing the results of σ to those observed in ceramic LSCO systems, assuming that m^* is independent of doping, the results for LCO:4.11 and LSCO:0.12 correspond to volume average hole densities of $\sim 0.14 +/- 0.02$ and $0.10 +/- 0.02$ holes per Cu, respectively. In view of the large systematic errors, however, we cannot use these results to distinguish whether the volume without static magnetism $(1-V_{Cu})$ alone or the total volume carries superconductivity. We can rule out, however, a case where superconducting carriers exist only in the magnetic volume V_{Cu}, since the local hole-concentration for this model would need to be unrealistically large (more than 0.3 holes per Cu) to account for the observed value of volume integrated n_s/m^*, which is comparable to those in LSCO systems in the optimum-doping region. So far, a clear indication of mutually exclusive regions with static magnetism and superconductivity has been obtained only in μSR measurements in $(La,Eu,Sr)_2CuO_4$ (LESCO),[40,54,55] which demonstrate that the superfluid density n_s/m^* scales as $(1-V_\mu)$.

In previous work on $La_{1.45}Nd_{0.4}Sr_{0.15}CuO_4$ and $La_{1.45}Nd_{0.4}Sr_{0.2}CuO_4$,[38] which are superconducting below $T_c \sim 7$ and 12 K, respectively, $V_\mu \sim 100\%$ was found. This result could be interpreted as evidence of spatial overlap of regions supporting superconductivity and regions having static spin order. The relationship in Fig. 8(a), however, in-

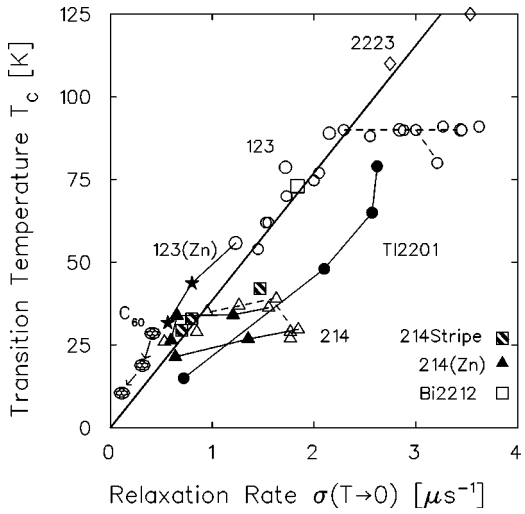

FIG. 14. A plot of the superconducting transition temperature T_c versus the relaxation rate $\sigma(T\rightarrow 0)$ at low temperatures (proportional to the superfluid density n_s/m^*) for several high-T_c superconductors (Refs. 49–52). The results with the ''stripe square'' symbols represent points from LESCO (Refs. 54 and 55), LSCO:0.12, and LCO:4.11 in the order of increasing $\sigma(T\rightarrow 0)$. To account for difference between results for ceramic and single-crystal specimens, the values for σ for LCO:4.11 and LSCO:0.12 in the CT-I configuration were multiplied by 1/1.4.

dicates that V_{Cu} for this system can be smaller than 100%. This leaves open the possibility that superconductivity with reduced T_c survives in a small remaining volume fraction $(1-V_{\mathrm{Cu}})\sim 20\%$, while superconducting regions and regions with static magnetism are mutually exclusive.

The situation with magnetic islands, having length scales comparable to the in-plane superconducting coherence length, resembles the ''swiss cheese model''[52] for Zn-doped HTSC systems, where a nonsuperconducting region of comparable size is created around each Zn. This model was proposed based on the μSR results for the reduction of n_s/m^* as a function of Zn concentration,[52] and was recently confirmed by direct measurements of scanning tunnelling microscopy (STM).[57] The μSR results for overdoped HTSC systems can also be explained if one assumes spontaneous formation of hole-rich nonsuperconducting islands embedded into a sea of hole-poor superfluid.[55,58–60] The correlation between T_c and n_s/m^* survives in all these systems, as shown in Fig. 14. We note that similar microscopic heterogeneity in the superconducting state has also been found in recent STM measurements on underdoped Bi2212 systems.[61]

The T_c vs n_s/m^* correlations are robust against various perturbations in HTSC materials, such as those caused by Zn impurities, overdoped fermion carriers, and the formation of static magnetic islands, seen in the present work. This is analogous to the robustness of correlations between the superfluid transition temperature and the two-dimensional superfluid density in thin films of ^{4}He and ^{3}He/^{4}He adsorbed in porous and nonporous media.[62–66] Based on these observations, one of us[55,59,60] pointed out a possible relevance of these heterogeneous electronic/magnetic features in HTSC systems to a ''microscopic phase separation,'' such as the one seen in superfluid ^{3}He/^{4}He films adsorbed in porous media / fine powders.[66,67]

In the present work on LCO:4.11, as well as a previous μSR study on LCO:4.02 and LCO4.04,[43] the onset of superconductivity occurs around the temperature below which the volume fraction of static magnetism increases with decreasing temperature. This apparent coincidence of T_c and T_N could be expected if a microscopic rearrangement of charge distribution occurs at $T_c\sim T_N$ to separate the electron systems into hole-rich regions which support superconductivity and hole poor ($x\sim 1/8$ for LCO:4.11 and $x\sim 0$ for LCO:4.02 and LCO:4.04) regions which support static magnetism.

Recently, Kivelson *et al.*[68] have proposed a model with a particular type of phase separation to explain the sharp rise of ν and gradual increase of V_{Cu} below T_N seen in the present study of LCO:4.11. Their model also predicts a trade off of superconducting and magnetic volumes below $T_c\sim T_N$. The gradual change of both $\sigma(T)$ and $V_\mu(T)$ below $T_c\sim T_N$ in LCO:4.11 [Figs. 3(a) and 13], however, seems inconsistent with such a trade off.

The superconducting T_c and the magnetic T_N appear at different temperatures in μSR measurements of LSCO:0.12 as well as in various LNSCO and LESCO systems, with LSCO:0.12 having $T_c>T_N$ and the other materials having $T_N>T_c$. It should be noted that neutron measurements give $T_c\simeq T_N$ in LSCO:0.12, while T_N determined by μSR is lower, presumably due to difference in time windows between neutron and muon measurements. In these systems the frequency ν increases with decreasing temperature gradually below T_N, as shown in Fig. 3(b), and in Refs. 38–42. Thus, the abrupt development of the magnetic order parameter is not a common feature of all the HTSC systems.

B. Bragg peak intensity in LCO:4.11 and AF-LCO

We can estimate the Bragg peak intensity $I_{B:4.11}$ expected in neutron scattering measurements on LCO:4.11 from the μSR results. $I_{B:4.11}$ should be reduced from the value $I_{B:\mathrm{AF}}$ in AF-LCO by a factor 0.5 for the SDW amplitude ($\sin^2$) times the ratio of the maximum static moments $(0.36/0.55)^2$ times the volume fraction of magnetic Cu atoms $V_{\mathrm{Cu}}=0.27$. Thus, we predict as a rough estimate $I_{B:4.11}=0.06I_{B:\mathrm{AF}}$. This value agrees well with the observed neutron results $I_{B:4.11}=0.07I_{B:\mathrm{AF}}$. In Ref. 16 it is assumed that three out of four copper ions are magnetic and that they are distributed uniformly throughout the entire volume, so a smaller average moment per Cu^{2+} of $0.15\mu_B$ is inferred.

We note, however, that estimates of the ordered moment size from neutron studies and from μSR often disagree with one another. For example, the Néel temperature in antiferromagnetic $La_2CuO_{4+\delta}$ varies from $T_N\sim 300$ K to $T_N\leqslant 100$ K with a small variation in δ. In neutron scattering studies of these AF-LCO systems, the Bragg peak intensity I_B shows a reduction, by more than a factor of 10, with decreasing T_N.[28] In contrast, the frequency of ZF-μSR spectra shows only a 20% change in the local frozen moment for the same reduction of T_N. These μSR and neutron results on AF-LCO are compared in Ref. 28. Since the μSR frequency

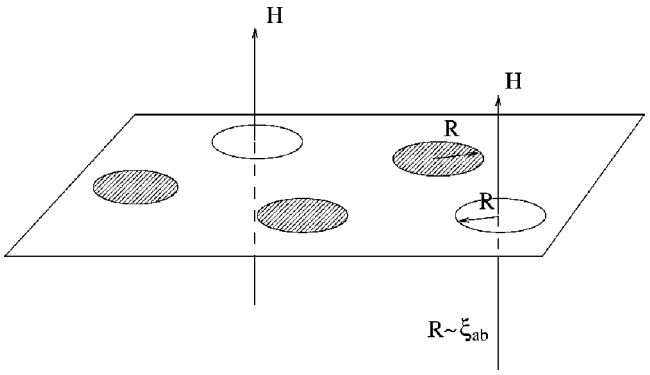

FIG. 15. An illustration of magnetic islands (shaded circles) and vortex cores (open circles) on the CuO_2 planes of HTSC systems under an external magnetic field applied along the *c* axis direction. When a core is located at the magnetic island, one expects an increase in the radius of the nonsuperconducting region due to supercurrent flowing around such a magnetic island.

is directly proportional to the magnitude of neighboring static Cu moments, the reduction of I_B in neutron studies cannot be ascribed to a change of individual Cu moment size. The likely reason for the strong reduction of I_B is a progressive trade off between the true long range ordered component and short range spin glass fluctuations which recent work[69] has shown involves fluctuations into the diagonal stripe spin glass phase with hole concentration of ~ 0.02.

C. Neutron results in high magnetic fields

Recently Khaykovich *et al.*[44] have made measurements on LCO:4.11 in high magnetic fields $H_{\rm ext}$ applied parallel to the *c* axis. By increasing the external field from $H_{\rm ext}=0$ to $H_{\rm ext}=9$ T, they have found a factor ~ 2 increase of the intensity I_B of the magnetic Bragg peak at $T\rightarrow 0$ for a crystal similar to the one studied here. The superconducting T_c is suppressed by $H_{\rm ext}$, while T_N remains nearly unchanged up to $H_{\rm ext}=9$ T. A similar increase of Bragg peak intensity in high fields was also observed by Katano *et al.*[70] in LSCO:0.12.

Application of $H_{\rm ext}$ perpendicular to the CuO_2 plane creates vortices. The vortex core, with radius comparable to the in-plane coherence length $\xi_{ab}\sim 30$ Å becomes normal, as illustrated in Fig. 15. These normal cores could have static magnetic order similar to that in the surrounding magnetic islands.

The fraction of the area contained in vortex cores may be estimated from the upper critical field, since that is the field at which the cores fill the entire area. Using $H_{c2}\geqslant 40$ T, found for optimally doped LSCO,[71] we expect that only $\sim 1/4$ or less of the area that is superconducting at $H_{\rm ext}=0$ would be turned into a normal core at $H_{\rm ext}=9$ T in LCO:4.11. However, this is sufficient to explain the factor ~ 2 increase in the Bragg peak intensity if the zero-field sample has ordered moments in only $\sim 27\%$ of its volume and if the magnetism in the cores is coherent with the long range order present at zero field. We are currently undertaking μSR studies of LCO:4.11 in high applied magnetic fields, which will be reported in future publications.

In nearly optimally doped LSCO, Lake *et al.*[72] have recently found that low-energy neutron scattering intensity, below the energy transfer corresponding to the superconducting energy gap, increases at temperatures well below T_c, when a high external field $H_{\rm ext}$ is applied along the *c* axis. This phenomenon may also be related to the magnetic response from the flux-core regions, since the increase of the intensity sets in at the flux-depinning temperature. A rather surprising feature of this study is the sharpness of the observed low-energy fluctuations in momentum space, suggesting long-range spin correlations among widely separated vortex core regions. We point out here that, similar to the static order, this requires long range coupling between vortex cores.

D. Conclusions

In summary, we have performed ZF-μSR measurements using LCO:4.11 and LSCO:0.12 single crystals, and have found that static incommensurate SDW spin freezing, with the maximum ordered Cu moment size of $0.36\mu_B$, develops only in a partial site fraction. We assume $V_\mu\sim 40\%$ for LCO:4.11 and $\sim 18\%$ for LSCO:0.12, and specific modeling suggests that the corresponding ordered Cu fractions may be somewhat smaller. Comparison of observed results with computer simulation suggests the formation of static magnetic islands on the CuO_2 planes having size $R=15$–30 Å, comparable to the in-plane superconducting coherence length ξ_{ab}. Order between these islands nevertheless propagates over long distances to yield a correlation length in excess of 600 Å.

We stress that LCO:4.11, which is a stoichiometric single crystal, has the least built-in randomness among the various HTSC systems that exhibit static incommensurate magnetic correlations. Yet the present work demonstrates that the ground state is a mixture of magnetically ordered and at best weakly ordered regions. Near phase boundaries or quantum critical points in strongly correlated electron systems, such microscopic heterogeneity could result from competition of the different order parameters involved. Related phenomena have been observed, for example, in the formation of stripe magnetic correlations in manganites[73] and the development of stripe domains in LSCO with $x\sim 0.01$ to 0.02.[74] These observations encourage further theoretical studies of electronic states involving spontaneous formation of heterogenous regions in competing order parameter systems.

Our TF-μSR measurements in these systems demonstrate that n_s/m^* at $T\rightarrow 0$ exhibits correlations with T_c not only in underdoped, Zn-doped, and overdoped HTSC systems but also in the present systems with static SDW spin freezing. Recent measurements of the penetration depth in $(BEDT\text{-}TTF)_2Cu(NCS)_2$ in applied pressure,[75] and in A_3C_{60} systems,[76,77] suggest that these correlations are followed also by organic and fullerine superconductors.

We have proposed a model for explaining the rather long-range spin correlations in these systems, resorting to ''connectivity'' of neighboring magnetic islands on the same and adjacent CuO_2 planes. We have also suggested that static magnetism in the vortex core region can provide explana-

tions for the field dependence of the neutron scattering results in LCO:4.11 and in optimally doped LSCO systems.

The present work demonstrates a very important feature of μSR, i.e., the capability to determine the volume fraction of magnetically ordered regions. Recently, a similar case was noticed in the study of URu_2Si_2, where static magnetism below $T_N \sim 17$ K has been identified to exist in a partial volume fraction by combination of neutron[78] and NMR (Ref. 79) studies in applied pressure. The first evidence for this feature was indeed provided by a μSR measurement[80] in ambient pressure. In the μSR results for URu_2Si_2, Luke *et al.* found a very sharp onset of the precession frequency $\nu(T)$ below T_N, temperature dependence of the precessing amplitude $V_\mu(T)$, and a good agreement between the temperature dependence $I_B(T)$ of the neutron Bragg peak and $V_\mu \nu^2$ from μSR. These features are common to the present results in LCO:4.11. We also note that ZF-μSR results in $CeCu_{2.2}Si_2$ (Refs. 81 and 82) indicate a possible trade off between magnetic and superconducting volume fractions. These results suggest possible involvement of microscopic phase separation in both HTSC systems and heavy fermion systems.[55,68,83] Further detailed studies of μSR in combination with neutron scattering will be very helpful in obtaining an overall understanding of the interplay between magnetism and superconductivity in HTSC, heavy-fermion, and other strongly correlated electron systems.

ACKNOWLEDGMENTS

We wish to acknowledge helpful discussions with B. Nachumi, G. Shirane, J.M. Tranquada, and S. Uchida. The work at Columbia was supported by NSF (Grant Nos. DMR-98-02000, DMR-01-02752, and CHE-01-17752) and US-Israel Binational Science Foundation. Research at McMaster was supported by NSERC and the Canadian Institute for Advanced Research. The work at MIT has been supported by the MRSEC Program of the National Science Foundation under Award No. DMR 9808941 and by NSF under Awards No. DMR-00-71256 and DMR-99-71264. Work at the University of Toronto is part of the Canadian Institute for Advanced Research and is supported by the Natural Science and Engineering Research Council of Canada. The research in Kyoto University was supported by the Japanese Ministry of Education, Culture, Sports, Science and Technology, Grant-in-Aid for Scientific Research on Priority Areas (Novel Quantum Phenomena in Transition Metal Oxides, Grant No. 12046239, 2001), for Research A (Grant No. 10304026, 2001), for Creative Scientific Research (Grant No. 13NP0201) ''Collaboratory on Electron Correlations—Toward a New Research Network between Physics and Chemistry'' and by the Japan Science and Technology Corporation, the Core Research for Evolutional Science and Technology Project (CREST).

*Author to whom correspondence should be addressed. Email address: tomo@lorentz.phys.columbia.edu

[1] For general review of magnetic and superconducting properties of HTSC systems, see, for example, M.A. Kastner, R.J. Birgeneau, G. Shirane, and Y. Endoh, Rev. Mod. Phys. **70**, 897 (1988).

[2] R.J. Birgeneau, Y. Endoh, K. Kakurai, Y. Hidaka, T. Murakami, M.A. Kastner, T.R. Thurston, G. Shirane, and K. Yamada, Phys. Rev. B **39**, 2868 (1989).

[3] Y. Endoh, K. Yamada, R.J. Birgeneau, D.R. Gabbe, H.P. Jenssen, M.A. Kastner, C.J. Peters, P.J. Picone, T.R. Thurston, J. M Tranquada, G. Shirane, Y. Hidaka, M. Oda, Y. Enomoto, M. Suzuki, and T. Murakami, Phys. Rev. B **37**, 7443 (1988).

[4] G. Shirane, R.J. Birgeneau, Y. Endoh, P. Gehring, M.A. Kastner, K. Kitazawa, H. Kojima, I. Tanaka, T.R. Thurston, and K. Yamada, Phys. Rev. Lett. **63**, 330 (1989).

[5] G. Aeppli, T.E. Mason, S.M. Hayden, H.A. Mook, and J. Kulda, Science **278**, 1432 (1997).

[6] H.A. Mook, P. Dai., K. Salama, D. Lee, F. Dogan, G. Aeppli, A.T. Boothroyd, and M.E. Mostoller, Phys. Rev. Lett. **77**, 370 (1996).

[7] H.A. Mook, P. Dai, S.M. Hayden, G. Aeppli, T.G. Perring, and F. Dogan, Nature (London) **395**, 580 (1998).

[8] M. Arai, T. Nishijima, Y. Endoh, T. Egami, S. Tajima, K. Tomimoto, Y. Shiohara, M. Takahashi, A. Garrett, and S.M. Bennington, Phys. Rev. Lett. **83**, 608 (1999).

[9] J.M. Tranquada, B.J. Sternlieb, J.D. Axe, Y. Nakamura, and S. Uchida, Nature (London) **375**, 561 (1995).

[10] J.M. Tranquada, J.D. Axe, N. Ichikawa, Y. Nakamura, S. Uchida, and B. Nachumi, Phys. Rev. B **54**, 7489 (1996).

[11] J.M. Tranquada, N. Ichikawa, and S. Uchida, Phys. Rev. B **59**, 14 712 (1999).

[12] K. Yamada, C.H. Lee, K. Kurahashi, J. Wada, S. Wakimoto, S. Ueki, H. Kimura, Y. Endoh, S. Hosoya, G. Shirane, R.J. Birgeneau, M. Greven, M.A. Kastner, and Y.J. Kim, Phys. Rev. B **57**, 6165 (1998).

[13] T. Suzuki, T. Goto, K. Chiba, T. Shinoda, T. Fukase, H. Kimura, K. Yamada, M. Ohashi, and Y. Yamaguchi, Phys. Rev. B **57**, R3229 (1998).

[14] S. Wakimoto, R.J. Birgeneau, Y.S. Lee, and G. Shirane, Phys. Rev. B **63**, 172501 (2001).

[15] B.O. Wells, Y.S. Lee, M.A. Kastner, R.J. Christianson, R.J. Birgeneau, K. Yamada, Y. Endoh, and G. Shirane, Science **277**, 1067 (1997).

[16] Y.S. Lee, R.J. Birgeneau, M.A. Kastner, Y. Endoh, S. Wakimoto, K. Yamada, R.W. Erwin, S.H. Lee, and G. Shirane, Phys. Rev. B **60**, 3643 (1999).

[17] A. Bianconi, A.C. Castellano, M. Desantis, P. Delogu, A. Gargano, and R. Giorgi, Solid State Commun. **63**, 1009 (1987).

[18] A. Bianconi, Physica C **235-240**, 269 (1994).

[19] A. Bianconi, N.L. Saini, T. Rossetti, A. Lanzara, A. Perali, M. Missori, H. Oyanagi, H. Yamaguchi, Y. Nishihara, and D.H. Ha, Phys. Rev. B **54**, 12 018 (1996).

[20] J. Zaanen and O. Gunnarsson, Phys. Rev. B **40**, 7391 (1989).

[21] D. Poilblanc and T.M. Rice, Phys. Rev. B **39**, 9749 (1989).

[22] V.J. Emery, S.A. Kivelson. and H.Q. Lin, Phys. Rev. Lett. **64**, 475 (1990).

[23] V.J. Emery, S.A. Kivelson, and O. Zachar, Phys. Rev. B **56**, 6120 (1997).

[24] For a general review of μSR, see, for example, A. Schenck, *Muon Spin Rotation Spectroscopy* (Adam Hilger, Bristol, 1985).

[25] For a recent reviews of μSR studies in topical subjects, see *Muon Science: Muons in Physics, Chemistry and Materials*, Proceedings of the *Fifty First Scottish Universities Summer School in*

Physics, St. Andrews, August, 1988, edited by S.L. Lee, S.H. Kilcoyne, and R. Cywinski (Institute of Physics Publishing, Bristol, 1999).

[26] A.T. Savici, Y. Fudamoto, I.M. Gat, M.I. Larkin, Y.J. Uemura, K.M. Kojima, Y.S. Lee, M.A. Kastner, and R.J. Birgeneau, Physica B **289-290**, 338 (2000).

[27] Y.J. Uemura, W.J. Kossler, X.H. Yu, J.R. Kempton, H.E. Schone, D. Opie, C.E. Stronach, D.C. Johnston, M.S. Alvarez, and D.P. Goshorn, Phys. Rev. Lett. **59**, 1045 (1987).

[28] Y.J. Uemura, W.J. Kossler, J.R. Kempton, X.H. Yu, H.E. Söeny, D. Opie, C.E. Stronach, J.H. Brewer, R.F. Kiefl, S.R. Kreitzman, G.M. Luke, T.M. Riseman, D.Ll. Williams, E.J. Ansaldo, Y. Endoh, Y. Kudo, K. Yamada, D.C. Johnston, M.S. Alvarez, D.P. Goshorn, Y. Hidaka, M. Oda, Y. Enomoto, M. Suzuki, and T. Murakami, Physica C **153-155**, 769 (1988).

[29] L.P. Le, R.H. Heffner, D.E. MacLaughlin, K. Kojima, G.M. Luke, B. Nachumi, Y.J. Uemura, J.L. Sarrao, and Z. Fisk, Phys. Rev. B **54**, 9538 (1996).

[30] D.R. Harshman, G. Aeppli, G.P. Espinosa, A.S. Cooper, J.P. Remeika, E.J. Ansaldo, T.M. Riseman, D.L. Williams, D.R. Noakes, B. Ellman, and T.F. Rosenbaum, Phys. Rev. B **38**, 852 (1988).

[31] B.J. Sternlieb, G.M. Luke, Y.J. Uemura, T.M. Riseman, J.H. Brewer, P.M. Gehring, K. Yamada, Y. Hidaka, T. Murakami, T.R. Thurston, and R.J. Birgeneau, Phys. Rev. B **41**, 8866 (1990).

[32] A. Weidinger, Ch. Niedermayer, A. Golnik, R. Simon, E. Recknagel, J.I. Budnick, B. Chamberland, and C. Baines, Phys. Rev. Lett. **62**, 102 (1989).

[33] F. Borsa, P. Carretta, J.H. Cho, F.C. Chou, Q. Hu, D.C. Johnston, A. Lascialfari, D.R. Torgeson, R.J. Gooding, N.M. Salem, and K.J.E. Vos, Phys. Rev. B **52**, 7334 (1995).

[34] Ch. Niedermayer, C. Bernhard, T. Blasius, A. Golnik, A. Moodenbaugh, and J.I. Budnick, Phys. Rev. Lett. **80**, 3843 (1998).

[35] J.H. Brewer, E.J. Ansaldo, J.F. Carolan, A.C.D. Chaklader, W.N. Hardy, D.R. Harshman, M.E. Hayden, M. Ishikawa, N. Kaplan, R. Keitel, J. Kempton, R.F. Kiefl, W.J. Kossler, S.R. Kreitzman, A. Kulpa, Y. Kuno, G.M. Luke, H. Miyatake, K. Nagamine, Y. Nakazawa, N. Nishida, K. Nishiyama, S. Ohkuma, T.M. Riseman, G. Roehmer, P. Schleger, D. Shimada, C.E. Stronach, T. Takabatake, Y.J. Uemura, Y. Watanabe, D.L. Williams, T. Yamazaki, and B. Yang, Phys. Rev. Lett. **60**, 1073 (1988).

[36] G.M. Luke, L.P. Le, B.J. Sternlieb, W.D. Wu, Y.J. Uemura, J.H. Brewer, T.M. Riseman, S. Isibashi, and S. Uchida, Physica C **185-189**, 1175 (1991).

[37] K. Kumagai, K. Kawano, I. Watanabe, K. Nishiyama, and K. Nagamine, Hyperfine Interact. **86**, 473 (1994).

[38] B. Nachumi, Y. Fudamoto, A. Keren, K.M. Kojima, M. Larkin, G.M. Luke, J. Merrin, O. Tchernyshyov, Y.J. Uemura, N. Ichikawa, M. Goto, H. Takagi, S. Uchida, M.K. Crawford, E.M. McCarron, D.E. MacLaughlin, and R.H. Heffner, Phys. Rev. B **58**, 8760 (1998).

[39] W. Wagener, H.H. Klauss, M. Hillberg, M.A.C. de Melo, M. Birke, F.J. Litterst, E. Schreier, B. Buchner, and H. Micklitz, Hyperfine Interact. **105**, 107 (1997).

[40] K.M. Kojima, H. Eisaki, S. Uchida, Y. Fudamoto, I.M. Gat, A. Kinkhabwara, M.I. Larkin, G.M. Luke, and Y.J. Uemura, Physica B **289**, 373 (2000).

[41] H.H. Klauss, W. Wagener, M. Hillberg, W. Kopmann, H. Walf, F.J. Litterst, M. Hücker, and B. Büchner, Phys. Rev. Lett. **85**, 4590 (2000).

[42] A. Lappas, K. Prassides, F.N. Gygax, and A. Schenck, J. Phys.: Condens. Matter **12**, 3401 (2000).

[43] V.Yu. Pomjakushin, A.A. Zakharov, A.M. Balagurov, F.N. Gygax, A. Schenck, A. Amato, D. Herlach, A.I. Beskrovny, V.N. Duginov, Yu.V. Obukhov, A.N. Ponomarev, and S.N. Barilo, Phys. Rev. B **58**, 12 350 (1998).

[44] B. Khaykovich, Y.S. Lee, S. Wakimoto, K.J. Thomas, R. Erwin, S.-H. Lee, M.A. Kastner, and R.J. Birgeneau, cond-mat/0112505 (unpublished).

[45] L.P. Le, A. Keren, G.M. Luke, B.J. Sternlieb, W.D. Wu, Y.J. Uemura, J.H. Brewer, T.M. Riseman, R.V. Upasani, L.Y. Chiang, W. Kang, P.M. Chaikin, T. Csiba, and G. Gruner, Phys. Rev. B **48**, 7284 (1993).

[46] L.P. Le, R.H. Heffner, J.D. Thompson, G.J. Nieuwenhuys, D.E. Maclaughlin, P.C. Canfield, B.K. Chyo, A. Amato, R. Feyerherm, F.N. Gygax, and A. Schenck, Hyperfine Interact. **104**, 49 (1997).

[47] B. Hitti, P. Birrer, K. Fischer, F.N. Gygax, E. Lippelt, H. Maletta, A. Schenck, and M. Weber, Hyperfine Interact. **63**, 287 (1990).

[48] J.E. Sonier, J.H. Brewer, and R.F. Kiefl, Rev. Mod. Phys. **72**, 769 (2002).

[49] Y.J. Uemura, G.M. Luke, B.J. Sternlieb, J.H. Brewer, J.F. Carolan, W.N. Hardy, R. Kadono, J.R. Kempton, R.F. Kiefl, S.R. Kreitzman, P. Mulhern, T.M. Riseman, D.Ll. Williams, B.X. Yang, S. Uchida, H. Takagi, J. Gopalakrishnan, A.W. Sleight, M.A. Subramanian, C.L. Chien, M.Z. Cieplak, Gang Xiao, V.Y. Lee, B.W. Statt, C.E. Stronach, W.J. Kossler, and X.H. Yu, Phys. Rev. Lett. **62**, 2317 (1989).

[50] Y.J. Uemura, L.P. Le, G.M. Luke, B.J. Sternlieb, W.D. Wu, J.H. Brewer, T.M. Riseman, C.L. Seaman, M.B. Maple, M. Ishikawa, D.G. Hinks, J.D. Jorgensen, G. Saito, and H. Yamochi, Phys. Rev. Lett. **66**, 2665 (1991).

[51] Y.J. Uemura, A. Keren, L.P. Le, G.M. Luke, W.D. Wu, Y. Kubo, T. Manako, Y. Shimakawa, M. Subramanian, J.L. Cobb, and J.T. Markert, Nature (London) **364**, 605 (1993).

[52] B. Nachumi, A. Keren, K. Kojima, M. Larkin, G.M. Luke, J. Merrin, O. Tchernyshov, Y.J. Uemura, N. Ichikawa, M. Goto, and S. Uchida, Phys. Rev. Lett. **77**, 5421 (1996).

[53] W. Barford and J.M.F. Gunn, Physica C **156**, 515 (1988).

[54] K.M. Kojima, T. Kakeshita, Y. Kojima, J. Tsukamoto, T. Ono, H. Eisaki, S. Uchida, Y. Fudamoto, I.M. Gat, M.I. Larkin, Y.J. Uemura, and G.M. Luke (unpublished).

[55] Y.J. Uemura, Physica C **341-348**, 2117 (2000).

[56] Ch. Niedermayer, C. Bernhard, U. Binninger, H. Glückler, J.L. Tallon, E.J. Ansaldo, and J.I. Budnick, Phys. Rev. Lett. **71**, 1764 (1993).

[57] S.H. Pan, E.W. Hudson, K.M. Lang, H. Eisaki, S. Uchida, and J.C. Davis, Nature (London) **403**, 746 (2000).

[58] Y.J. Uemura, Physica C **282-287**, 194 (1997).

[59] Y.J. Uemura, Int. J. Mod. Phys. B **14**, 3003 (2000).

[60] Y.J. Uemura, Solid State Commun. **120**, 347 (2001).

[61] S.H. Pan, J.P. O'Neal, R.L. Badzey, C. Chamon, H. Ding, J.R. Engelbrecht, Z. Wang, H. Eisaki, S. Uchida, A.K. Gupta, W.-W. Ng, E.W. Hudson, K.M. Lang, and J.C. Davis, Nature (London) **413**, 282 (2001).

[62] G. Agnolet, D.F. McQueeney, and J.D. Reppy, Phys. Rev. B **39**, 8934 (1989).

[63] D.J. Bishop, J.E. Berthold, J.M. Parpia, and J.D. Reppy, Phys. Rev. B **24**, 5047 (1981).
[64] K. Shirahama, M. Kubota, S. Ogawa, N. Wada, and T. Watanabe, Phys. Rev. Lett. **64**, 1541 (1990).
[65] P.A. Crowell, F.W. Van Keuls, and J.D. Reppy, Phys. Rev. B **55**, 12 620 (1997).
[66] H. Chyo and G.A. Williams, J. Low Temp. Phys. **110**, 533 (1998).
[67] M. Chan, N. Mulders, and J. Reppy, Phys. Today **49** (8), 30 (1996).
[68] S.A. Kivelson, G. Aeppli, and V.J. Emery, Proc. Natl. Acad. Sci. U.S.A. **98**, 11 903 (2001).
[69] M. Matsuda, M. Fujita, K. Yamada, R.J. Birgeneau, M.A. Kastner, H. Hiraka, Y. Endoh, S. Wakimoto, and G. Shirane, Phys. Rev. B **62**, 9148 (2000).
[70] S. Katano, M. Sato, K. Yamada, T. Suzuki, and T. Fukase, Phys. Rev. B **62**, R14 677 (2000).
[71] G.S. Boebinger, Y. Ando, A. Passner, T. Kimura, M. Okuya, J. Shimoyama, K. Kishio, K. Tamasaku, N. Ichikawa, and S. Uchida, Phys. Rev. Lett. **77**, 5417 (1996).
[72] B. Lake, G. Aeppli, K.N. Clausen, D.F. McMorrow, K. Lefmann, N.E. Hussey, N. Mangkorntong, M. Nohara, H. Takagi, T.E. Mason, and A. Schröder, Science **291**, 1759 (2001).
[73] E. Dagotto, T. Hotta, and A. Moreo, Phys. Rep. **344**, 1 (2001).
[74] M. Matsuda, M. Fujita, K. Yamada, R.J. Birgeneau, Y. Endoh, and G. Shirane, cond-mat/011228 (unpublished).
[75] M.I. Larkin, A. Kinkhabwala, Y.J. Uemura, Y. Sushko, and G. Saito, Phys. Rev. B **64**, 144514 (2001).
[76] Y.J. Uemura, A. Keren, G.M. Luke, L.P. Le, B.J. Sternlieb, W.D. Wu, J.H. Brewer, R.L. Whetten, S.m. Huang, Sophia Lin, R.b. Kaner, F. Diederich, S. Donnovan, G. Grüner, and K. Holczer, Nature (London) **352**, 605 (1991).
[77] Y.J. Uemura, A. Keren, L.P. Le, G.M. Luke, W.D. Wu, J.S. Tsai, K. Tanigaki, K. Holczer, S. Donovan, and R.L. Whetten, Physica C **235-240**, 2501 (1994).
[78] H. Amitsuka, M. Sato, N. Metoki, M. Yokoyama, K. Kuwahara, T. Sakakibara, H. Morimoto, S. Kawarazaki, Y. Miyako, and J.A. Mydosh, Phys. Rev. Lett. **83**, 5114 (1999).
[79] K. Matsuda, Y. Kohori, T. Kohara, K. Kuwahara, and H. Amitsuka, Phys. Rev. Lett. **87**, 087203 (2001).
[80] G.M. Luke, A. Keren, L.P. Le, Y.J. Uemura, W.D. Wu, D. Bonn, L. Taillefer, J.D. Garrett, and Y. Onuki, Hyperfine Interact. **85**, 397 (1994).
[81] Y.J. Uemura, W.J. Kossler, X.H. Yu, H.E. Schone, J.R. Kempton, C.E. Stronach, S. Barth, F.N. Gygax, B. Hitti, A. Schenck, C. Baines, W.F. Lankford, Y. Onuki, and T. Komatsubara, Phys. Rev. B **39**, 4726 (1989).
[82] G.M. Luke, A. Keren, K. Kojima, L.P. Le, B.J. Sternlieb, W.D. Wu, Y.J. Uemura, Y. Onuki, and T. Komatsubara, Phys. Rev. Lett. **73**, 1853 (1994).
[83] P. Chandra, P. Coleman, and J.A. Mydosh, cond-mat/0110048 (unpublished).